

# Elimination of PPG Signal Disturbances through Variational Mode Decomposition and Hilbert Transform

Thanh Trung Thai, Thanh Tung Luu\*, Khanh Duy Phan



Use your smartphone to scan this QR code and download this article

Department of Construction Machinery and Handling Equipment, Faculty of Mechanical Engineering, Ho Chi Minh City University of Technology (HCMUT, Vietnam

## Correspondence

**Thanh Tung Luu**, Department of Construction Machinery and Handling Equipment, Faculty of Mechanical Engineering, Ho Chi Minh City University of Technology (HCMUT, Vietnam

Email: luuthanhtung2002@gmail.com

## History

- Received: 03-3-2024
- Accepted: 04-7-2024
- Published Online:

## DOI :



## Copyright

© VNUHCM Press. This is an open-access article distributed under the terms of the Creative Commons Attribution 4.0 International license.



## ABSTRACT

The PPG signal presents considerable promise as a non-invasive technique across various applications. However, effectively utilizing this signal in real-world scenarios demands meticulous handling to identify and rectify disturbances within the photo-plethysmography (PPG) signal. Among the methodologies explored, integrating time-frequency spectra with a hybrid deep learning model, such as convolutional – long short term memory neural network model (CNN-LSTM), has emerged as a promising approach. Yet, prevalent methods often rely on Fourier-based algorithms for extracting time-frequency spectra, which are prone to energy leakage issues. To surmount this limitation, decomposition methods like Variational Mode Decomposition (VMD) coupled with the Hilbert transform offer a compelling solution. In this study, we propose a novel algorithm leveraging VMD and Hilbert transform to extract time-frequency spectra as features for a convolutional neural network model (CNN). Unlike studies employing Fourier-based time-frequency spectra and the hybrid CNN-LSTM model, this approach adopts a simpler architecture, relying solely on a CNN model. This simplicity owes to the efficacy of VMD and Hilbert transform in feature extraction, streamlining the computational process without sacrificing accuracy. Remarkably, our method yields high-performance outcomes, achieving accuracy, precision, and recall of 0.91, 0.95, 0.88, respectively on the MIMICIII dataset. These results underscore the robustness and effectiveness of our proposed methodology, offering promising avenues for enhanced utilization of the PPG signal in diverse biomedical applications. By amalgamating advanced signal processing techniques with deep learning models, our approach contributes to the advancement of non-invasive biomedical signal processing, potentially healthcare monitoring and diagnosis.

**Key words:** photo-plethysmography, photo-plethysmography signal processing

## 1 INTRODUCTION

2 Photoplethysmography (PPG) is a non-invasive technique that is used to detect blood volume variations through an infrared light sensor placed on the surface of the skin<sup>1,2</sup>. Correct identification of the PPG waveform and its main features is essential in order to extract several biomarkers, such as heart rate, blood pressure, cardiac output, and blood oxygen saturation, when the red and infrared light are used simultaneously<sup>1,3</sup>. However, the practical application of PPG encounters difficulties as this signal is easily influenced by users' movements. Consequently, the identification and removal of disturbed PPG segments within the overall signal are crucial.

15 The initial and most basic technique for assessing the PPG signal involves the Signal Quality Index (SQI). This approach partitions the PPG signal into multiple segments, subsequently computing the SQI for each segment. A segment is deemed to be of high quality if its SQI value exceeds a predefined threshold<sup>4</sup>.

21 The foundation of this method relies on the observation that PPG signal waveforms undergo periodic

changes, consequently, the SQI associated with these signals is expected to exhibit a specific distribution pattern<sup>5</sup>. Figure 1 indicates the disparity in kurtosis and skewness distribution between quality and poor-quality PPG signal. However, a drawback of the SQI method lies in the multitude of proposed quality indices. Despite Elgendi's survey,<sup>6</sup> favoring "skewness" as the optimal index, establishing a universal threshold for these indices remains challenging.

The application of deep learning models can address the limitations of the SQI method by employing a deep model to learn the distinguishing features of high-quality PPG signals. Li et al.<sup>7</sup> utilized the Dynamic Time Warping (DWT) technique and a multi-layer perceptron model to evaluate PPG signal. This method was proposed to address physiological blood flow variations, leading to changes in the morphology of PPG signals. Esgalhadó et al.<sup>8</sup> conducted a survey on deep learning models to eliminate poor-quality PPG signal segments. The study compared Long Short-Term Memory (LSTM), Bidirectional LSTM, and Convolutional Neural Network (CNN) models.

**Cite this article :** Thai T T, Luu T T, Phan K D. **Elimination of PPG Signal Disturbances through Variational Mode Decomposition and Hilbert Transform.** *Sci. Tech. Dev. J. – Engineering and Technology* 2024; (1):1-8.

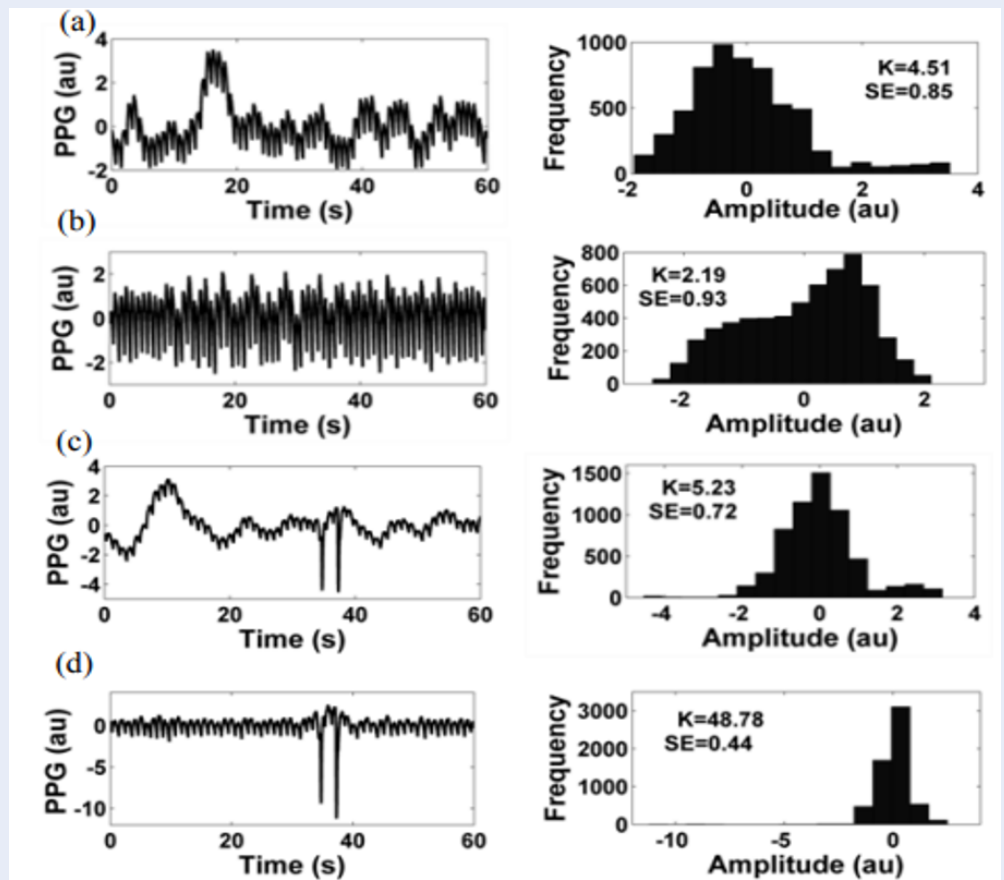


**Figure 1:** Sample clean (a-b) and corrupted (c-d) ear-PPG segments applied with linear (a, c) and 32nd order polynomial detrends (b, d) are shown along with their respective histograms and calculated kurtosis (K) and Shannon entropy (SE) values. The higher-order polynomial detrending is critical to enhance the specificity in the presence of physiological baseline drift (a) and the sensitivity in the presence of artifacts (c),<sup>4</sup>.

45 Besides, they also considered about the input data  
 46 for the model. The research findings indicated that  
 47 the CNN-LSTM algorithm, with Synchrosqueezed  
 48 Fourier Transform (SSFT) input, demonstrated the  
 49 highest performance with accuracy, 0.894. To explain  
 50 the effectiveness of their approach, the authors ex-  
 51 plained that applying a time-frequency transform to  
 52 the signals before classification provided the model  
 53 with an expanded feature set. This extended dataset  
 54 also facilitates signal projection from the time to the  
 55 time-frequency domain, where non-stationary com-  
 56 ponents may be better represented. Similar stud-  
 57 ies utilizing comparable deep learning models can be  
 58 found in<sup>9</sup>.  
 59 It can be seen that deep learning model with a time-  
 60 frequency input is a good choice for detecting and  
 61 removing non-quality part in PPG signal. However,  
 62 Fourier based method like SSFT representations has  
 63 drawbacks regarding “energy leakage”<sup>10</sup>. This is a

phenomenon where energy regions of the signal have  
 low concentration density, leading to some errors in  
 CNN model processing. This drawback can be over-  
 come by a method using VMD and Hilbert transform  
 to create combined time-frequency spectra with CNN  
 networks to identify and eliminate PPG signal seg-  
 ments affected by user motion.

## MATERIALS-METHODS

### Generating time – frequency spectrum

Instead of employing SSFT as in prior research, this  
 study utilized VMD to decompose the raw PPG signal  
 into sub-signals known as Intrinsic Mode Functions  
 (IMFs). Subsequently, dominant IMFs were selected  
 to generate a time-frequency spectrum by using the  
 Hilbert transform. VMD, introduced by Dragomiret-  
 skiyyi et al.<sup>11</sup>, decomposes a signal into signals, called

80 Intrinsic Mode Functions (IMFs) in form:

$$IMF(t) = A(t) \cdot \cos(\phi(t)) \quad (1)$$

81 where A(t) is the amplitude over time,  $\phi(t)$  is the fre-  
82 quency over time.

83 VMD determine the central frequency band of each  
84 IMF and proceed to analyze the original signal into  
85 IMFs with frequency domains around the central fre-  
86 quency. By pre-defining the number k of IMFs that  
87 the signal can have, computing the IMF channels is  
88 performed by a recursive loop:

89 In the  $(n+1)^{th}$  iteration, the  $k^{th}$  IMF is computed as  
90 follows:

$$U_k^{n+1}(f) = \frac{x(f) \sum_{i < k} U_k^{n+1}(f) - \sum_{i > k} U_k^n(f) + \wedge^n(f)}{1 + 2\alpha \{2\pi(f - f_k^n)\}^2} \quad (2)$$

91  $U_k^{n+1}(f)$  is the Fourier transform of the  $k^{th}$  IMF in  
92 the  $(n+1)^{th}$  iteration.

93 Along with that, the central frequency and the La-  
94 grange multiplier are also updated.

95  $k^{th}$  central frequency,  $f_k^{n+1}$ :

$$f_k^{n+1} = \frac{\int_0^\infty |U_k^{n+1}(f)|^2 f df}{\int_0^\infty |U_k^{n+1}(f)|^2 df} \approx \frac{\sum f |U_k^{n+1}(f)|^2}{\sum |U_k^{n+1}(f)|^2} \quad (3)$$

96 Lagrange multiplier:

$$\wedge^{n+1}(f) = \wedge^n(f) + \tau (X(f) - \sum_k U_k^{n+1}(f))$$

97 where  $\tau$  is the update rate of the coefficient Larrange.

98 When the algorithm satisfies the following condition,  
99 the loop stops:

$$\begin{cases} \sum_k \frac{\|u_k^{n+1}(t) - u_k^n(t)\|_2^2}{\|u_k^n(t)\|_2^2} < \epsilon_r \\ \sum_k \|u_k^{n+1}(t) - u_k^n(t)\|_2 < \epsilon_a \end{cases} \quad (4)$$

100 In this work, the PPG signal was decomposed into  
101 IMF channels through the VMD, with the algorithm's  
102 parameters as follows:

103 *Number of IMF channels*

104 The number of IMF channels used in this study does  
105 not fix. Instead, for each PPG signal, the number of  
106 IMF channels is automatically adjusted based on the  
107 independence of IMF channels from each other us-  
108 ing the covariance matrix<sup>12</sup>. When the determinant

109 of the matrix is above 0.8, the parameters are selected.

110 *Stopping criteria parameters*

$$\begin{cases} \epsilon_a = 5.10^{-6} \\ \epsilon_r = 5.10^{-3} \end{cases} \quad (5)$$

The IMFs which were decomposed from the raw PPG  
111 signal will be used to generate time-frequency spec-  
112 trum by using Hilbert transform. This transform de-  
113 fines an analytic signal as:  
114

$$z(t) = x(t) + i \cdot y(t) \quad (6)$$

$$y(t) = \frac{1}{\pi} P \int_{-\infty}^{+\infty} \frac{x(\tau)}{t - \tau} d\tau \quad (7)$$

Where  $x(t)$  is the IMF,  $y(t)$  is the Hilbert transform  
115 of  $x(t)$ , P is the Cauchy principle. Then the time-  
116 frequency spectrum is:  
117

$$H(f_0, t_0) = \sum_{i, f_i(t_0)}^N = f_0 a_i(t_0) \quad (8)$$

For each coordinate  $(t_0, f_0)$  in the spectrum, the spec-  
118 trum value is the sum of all amplitudes of all IMFs at  
119 time  $t_0$  with the respective frequency equal to  $f_0$ .

Where  $f, t$  are frequency and time point of interest,  $a(t)$   
121 is the instantaneous amplitude at time,  $t$ ,  $f(t)$  is the in-  
122 stantaneous frequency at time,  $t$ . The instantaneous  
123 amplitude and frequency of each IMF are calculate as  
124 follow:  
125

*The instantaneous amplitude*  
126

$$a(t) = \sqrt{x^2(t) + y^2(t)} \quad (9)$$

*The instantaneous frequency*  
127

$$f(t) = \frac{1}{2\pi} \frac{d}{dt} \left[ \arctan \frac{y(t)}{x(t)} \right] \quad (10)$$

Another advantage in implementing VMD and  
128 Hilbert transform is to filter out frequency band noise  
129 of signal without affect to the purity of original sig-  
130 nal. This is conducted via chosen IMFs with central  
131 frequency regions ranging from 0.5Hz to 3Hz. The  
132 central frequency region is determined based on the  
133 mean and standard deviation of the instantaneous fre-  
134 quency of that IMF, specifically.  
135

*The average instantaneous frequency*  
136

$$\bar{f} = \frac{1}{T} \int_0^T f(t) dt \quad (11)$$

*Standard deviation of the instantaneous frequency*  
137

$$\bar{s} = \sqrt{\frac{1}{T} \int_0^T (f(t) - \bar{f})^2 dt} \quad (12)$$

Then the central frequency range will be  
138  $(\bar{f} - \bar{s}, \bar{f} + \bar{s})$ .  
139

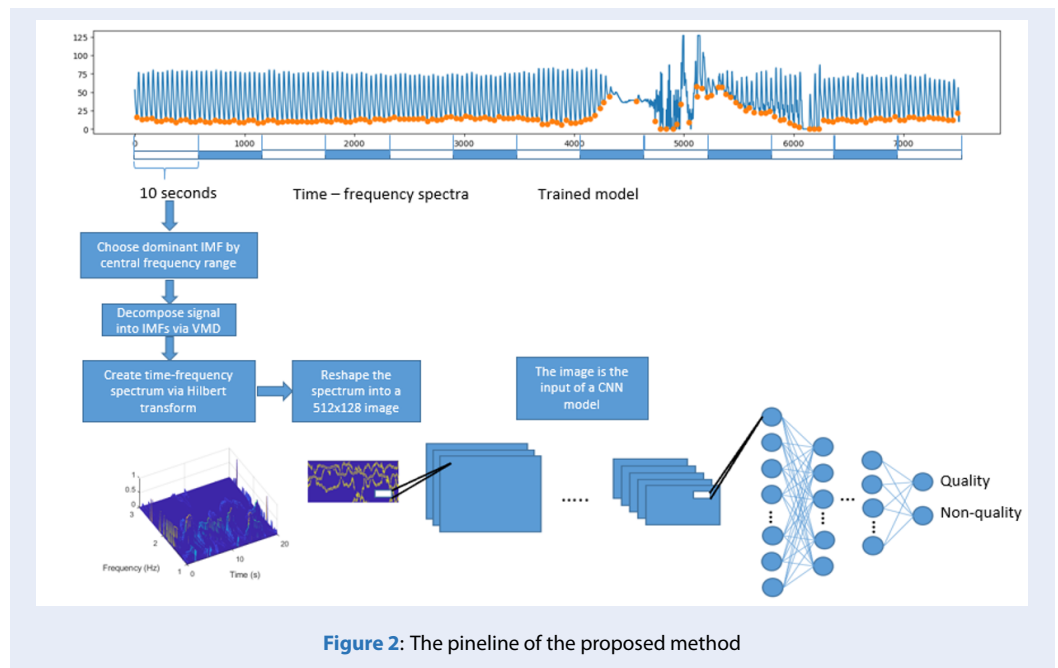


Figure 2: The pipeline of the proposed method

140 **Proposed method**

141 As mentioned earlier, the proposed methodology in  
 142 this study relied on VMD and the Hilbert transform  
 143 in conjunction with a CNN model. The pipeline illus-  
 144 trating the entire process is depicted in Figure 2.

145 Given the typical requirement of approximately 10  
 146 seconds of data length for most PPG signal applica-  
 147 tions, the raw PPG signal was segmented into 10-  
 148 second segments with 1-second padding at both the  
 149 start and end. Each segment underwent decomposi-  
 150 tion into Intrinsic Mode Functions (IMFs) using Vari-  
 151 ational Mode Decomposition (VMD). The mean and  
 152 standard deviation of the instantaneous frequency of  
 153 each IMF were computed to establish the central fre-  
 154 quency range. An IMF exhibiting a central frequency  
 155 range between 0.5Hz and 3Hz was selected as the  
 156 dominant IMF. The dominant IMFs were utilized to  
 157 construct a time-frequency spectrum via the Hilbert  
 158 transform. Subsequently, the 1-second padding at the  
 159 spectrum’s beginning and end was removed to miti-  
 160 gate the ‘end effect’ inherent in the Hilbert transform.  
 161 The resulting spectrum was reshaped into a image.  
 162 This image served as input for a CNN model designed  
 163 to assess the quality of the PPG signal. The architec-  
 164 ture of this model is detailed in Table 1. The entire  
 165 method was implemented using the PyTorch frame-  
 166 work and Python programming language.

167 **Dataset**

168 This study obtained PPG data from a cohort of sub-  
 169 jects sourced from the open source MIMIC-III wave-

form database<sup>13</sup>. Each PPG signal in the dataset was  
 170 segmented into 10-second segments with 1-second  
 171 padding and labeled as either “good” or “not good”  
 172 via the criteria from study of Elgendi et al.<sup>6</sup>. Figure 3  
 173 depicts the classify of PPG signal.

174  
 175 The training process utilized data from only 80% of  
 176 the PPG segments in the MIMIC-III dataset. A de-  
 177 tailed statistical description of the data is presented in  
 178 Table 2.

179 **METRIC**

180 The model is evaluated based on its precision, accu-  
 181 racy, and recall, as most studies in this field have em-  
 182 ployed. The calculation formulas for these criteria are  
 183 as follows:

184 *Precision*

$$Pre = \frac{TP}{TP + FP} \tag{13}$$

185 *Recall*

$$Re = \frac{TP}{TP + FN} \tag{14}$$

186 *Accuracy*

$$Acc = \frac{TP + TN}{FP + TP + TN + FN} \tag{15}$$

187 TP: The number of samples that are correctly classified  
 188 as positive instances (i.e., the model predicts positive  
 189 and the actual class is positive).

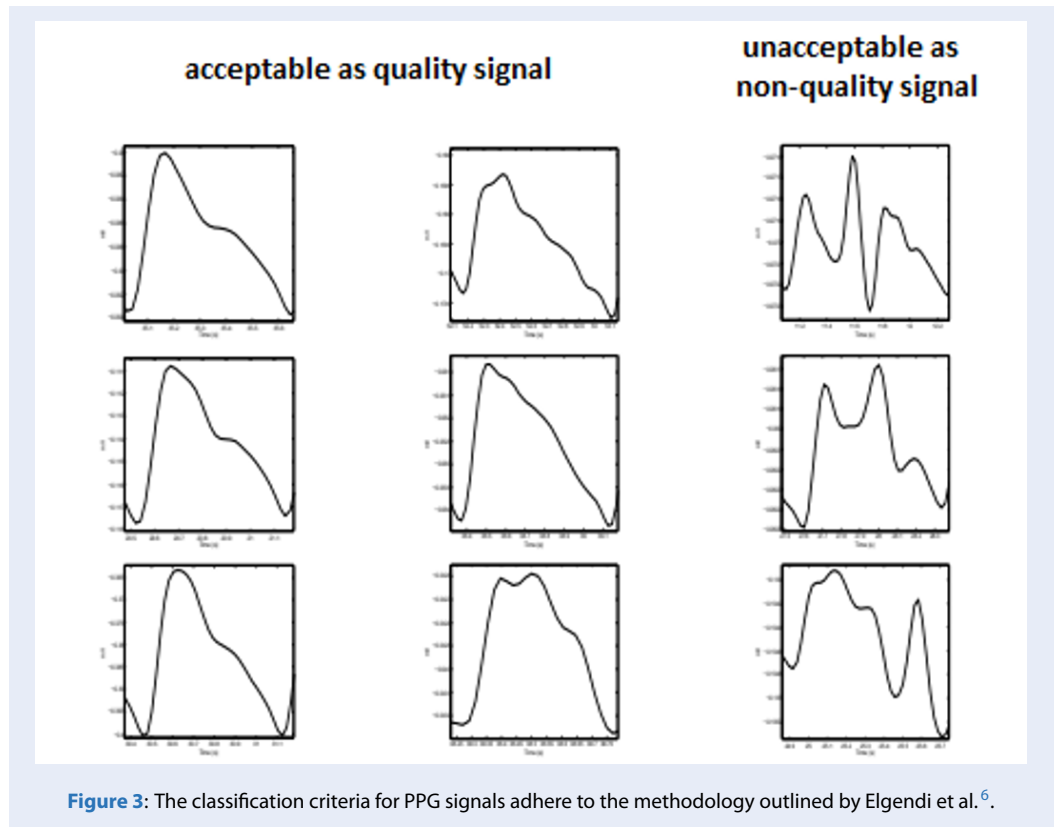
190 TN: The number of samples that are correctly classi-  
 191 fied as negative instances (i.e., the model predicts nega-  
 192 tive and the actual class is negative).

**Table 1: Structure of the model**

Layer	Type	Kernel	Strike	Channels	Shape
1	CNV	5×9	1	8	128×512×3
	LeakyReLU	-	-	-	128×512×8
	MAX	5×9	1	-	128×512×8
2	CNV	5×9	1	8	128×512×8
	LeakyReLU	-	-	-	128×512×8
	MAX	5×9	2	-	128×512×8
3	CNV	5×9	1	8	64×256×8
	LeakyReLU	-	-	-	64×256×16
	MAX	5×9	1	-	64×256×16
4	CNV	5×9	1	16	64×256×16
	LeakyReLU	-	-	-	64×256×16
	MAX	5×9	2	-	64×256×16
5	CNV	3×5	1	16	32×128×16
	LeakyReLU	-	-	-	32×128×16
	MAX	3×5	2	-	32×128×16
6	CNV	1×3	1	16	16×64×16
	LeakyReLU	-	-	-	16×64×16
	MAX	3×5	2	-	16×64×16
7	CNV	1×3	1	16	8×32×16
	LeakyReLU	-	-	-	8×32×16
	MAX	3×5	2	-	8×32×16
8	Fully connected layer	-	-	256	1024
9	Fully connected layer	-	-	-	256
10	Fully connected layer	-	-	-	150
11	Output	-	-	-	2

**Table 2: Statistical description of the data.**

MIMIC	140 subjects	
Total segment	3500 segments	
	Quality	Non - quality
Training set	912	1187
Validation set	316	383
Test set	354	346



193 FP: The number of samples that are incorrectly classi-  
 194 fied as positive instances (i.e., the model predicts posi-  
 195 tive but the actual class is negative).  
 196 FN: The number of samples that are incorrectly classi-  
 197 fied as negative instances (i.e., the model predicts neg-  
 198 ative but the actual class is positive).

199 **RESULT**

200 The training process consists of 45 epochs with a batch  
 201 size of 512, learning rate of 0.0001. Figure 4 and Fig-  
 202 ure 5 illustrate the training and validation accuracy  
 203 for each epoch. It is evident that the loss and accuracy  
 204 values for both datasets are closely aligned, indicating  
 205 the absence of overfitting.

206 The identification results for the test set demonstrate  
 207 high performance. As shown in Table 3, the confu-  
 208 sion matrix indicates an accuracy of 0.91, a precision  
 209 of 0.95, and a recall of 0.88.

210 **DISCUSSION**

211 Compared to other time-frequency spectrum and  
 212 deep model-based approaches, the proposed method  
 213 achieves similar high performance with a simpler  
 214 deep model. This advantage contributes to its imple-  
 215 mentation for applications on edge devices. Esgal-  
 216 hado et al.<sup>8</sup> utilized a hybrid CNN-LSTM model with



SSFT time-frequency spectrum input and achieved  
 performance with accuracy 0.89, precision 0.92, and  
 recall 0.91. In contrast, the proposed method only  
 employed CNN and demonstrated comparable per-  
 formance in terms of accuracy 0.91, precision 0.95,  
 and recall 0.88. This disparity can be attributed to  
 differences in time-frequency spectrum generation  
 methods. Fourier-based methods, such as SSFT used  
 in<sup>8</sup>, exhibit energy leakage phenomena. This leads  
 to less dense spectra, necessitating more complex  
 models to enhance sparsity at each layer for accu-



**Table 3: Confusion matrix of the proposed method's result on test set.**

Confusion matrix		True class	
		Positive	Negative
Predicated class	Positive	TP = 339	FP = 15
	Negative	FN = 44	TN = 302

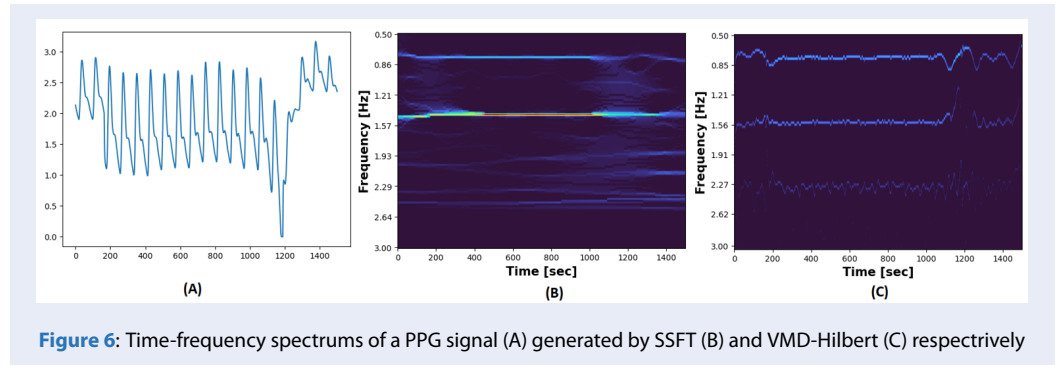


**Figure 6: Time-frequency spectrums of a PPG signal (A) generated by SSFT (B) and VMD-Hilbert (C) respectively**

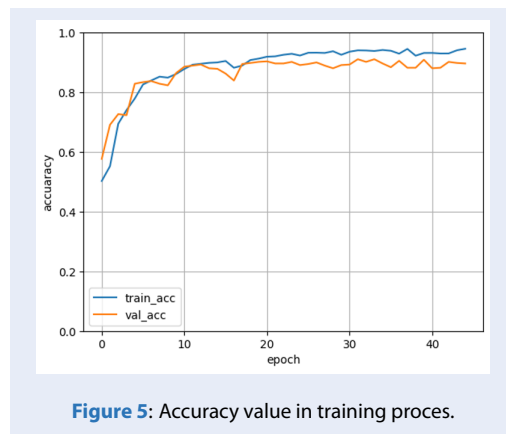


**Figure 5: Accuracy value in training proces.**

228 rate processing. Conversely, time-frequency spectra  
 229 from VMD and Hilbert transform offer denser spec-  
 230 tra, enabling simpler models to handle them more  
 231 effectively. Figure 6 illustrates time-frequency spec-  
 232 tra of the same PPG signal generated by SSFT and  
 233 VMD-Hilbert methods, respectively. Upon initial  
 234 inspection, the signal exhibits two disturbance seg-  
 235 ments around sample 200 and sample 1200, both  
 236 of which are clearly depicted in both spectra with  
 237 chaotic frequency zones at the respective samples.  
 238 Moreover, there is a significant difference between  
 239 the two spectra, influencing their effectiveness as  
 240 model inputs. The spectrum generated by the VMD-  
 241 Hilbert method features three distinct frequency  
 242 modes around 0.84Hz, 1.56Hz, and 2.27Hz. In con-  
 243 trast, although also depicting two frequency modes  
 244 around 0.84Hz and 1.56Hz, the spectrum from SSFT

245 exhibits significant energy leakage with numerous  
 246 frequency zones, rendering the frequency mode at  
 247 2.27Hz nearly indistinct. The explanation for this  
 248 disparity lies in the VMD method, which decom-  
 249 poses the signal into individual modes, each repre-  
 250 senting a specific frequency zone while preserving  
 251 the signal's non-linear and continuous instantaneous  
 252 frequency characteristics. Due to its ability to sep-  
 253 arate frequency modes distinctly, it becomes easier  
 254 to eliminate unrelated components, such as those in-  
 255 duced by environmental noise, based on the central  
 256 frequency range mentioned earlier. This process en-  
 257 sures that the final spectrum retains only the domi-  
 258 nant frequency modes, revealing the essential aspects  
 259 of the signal. In contrast, the SSFT analyzes the entire  
 260 signal directly from the raw data. While the imple-  
 261 mentation of a bandpass filter can mitigate this issue,  
 262 it risks eliminating crucial signal features, as noted  
 263 in<sup>14</sup>. Additionally, employing the Hilbert transform  
 264 for each IMF enhances independence between indi-  
 265 vidual IMFs. This independence contributes to the  
 266 density of the spectrum compared to SSFT, which  
 267 analyzes data along sliding windows without consid-  
 268 ering the independent nature of each frequency mode.

## CONCLUSION

269  
 270 This paper presents a method for identifying and re-  
 271 moving disturbed PPG segments. The algorithm's  
 272 key feature is based on the exceptional non-stationary  
 273 analysis capabilities of VMD and the Hilbert trans-  
 274 form. Despite the utilization of a deep model, it re-  
 275 mains simple enough to be applied in practice with  
 276 edge devices.  
 277

## 277 ACKNOWLEDGEMENTS

278 This research is funded by Department of Science  
279 and Technology under grant number 17/2023/HĐ-  
280 QKHCN. We acknowledge Ho Chi Minh City Univer-  
281 sity of Technology (HCMUT), VNU-HCM for sup-  
282 porting this study.

## 283 LIST OF ABBREVIATIONS

284 PPG: Photoplethysmography  
285 CNN: Convolutional neural network  
286 CNV: Convolution layer  
287 LSTM: Long short term memory  
288 SSFT: Synchrosqueezed Fourier Transform  
289 VMD: Variational Mode Decomposition  
290 IMF: Intrinsic Mode Function  
291 MAX: Max pooling layer

## 292 CONFLICTS OF INTERESTS

293 The authors declare no competing interests associated  
294 with the publication of this article.

## 295 AUTHORS' CONTRIBUTION

296 Thanh Trung Thai, Khanh Duy Phan: methodology,  
297 Thanh Tung Luu: supervision, analysis.

## 298 REFERENCES

- 299 1. Allen J. Photoplethysmography and its application in clinical  
300 physiological measurement. *Physiol Meas.* 2007;28(3) ;PMID:  
301 17322588. Available from: [https://doi.org/10.1088/0967-3334/](https://doi.org/10.1088/0967-3334/28/3/R01)  
302 [28/3/R01](https://doi.org/10.1088/0967-3334/28/3/R01).
- 303 2. Elgendi M. On the analysis of fingertip photoplethysmogram  
304 signals. *Curr Cardiol Rev.* 2012;8:14-25;PMID: 22845812. Avail-  
305 able from: <https://doi.org/10.2174/157340312801215782>.
- 306 3. Ram MR, Madhav KV, Krishna EH, Komalla NR, Reddy KA. A  
307 novel approach for motion artifact reduction in PPG signals  
308 based on AS-LMS adaptive filter. *IEEE Trans Instrum Meas.*  
309 2012;61:1445-57; Available from: [https://doi.org/10.1109/TIM.](https://doi.org/10.1109/TIM.2011.2175832)  
310 [2011.2175832](https://doi.org/10.1109/TIM.2011.2175832).
- 311 4. Selvaraj N, et al. Statistical approach for the detection of mo-  
312 tion/noise artifacts in photoplethysmogram. In: 2011 Annual  
313 International Conference of the IEEE Engineering in Medicine  
314 and Biology Society; 2011; Boston, MA, USA. IEEE; 2011. p.  
315 4972-5;PMID: 22255454. Available from: [https://doi.org/10.](https://doi.org/10.1109/IEMBS.2011.6091232)  
316 [1109/IEMBS.2011.6091232](https://doi.org/10.1109/IEMBS.2011.6091232).
- 317 5. Hanyu S, Xiaohui C. Motion artifact detection and reduction  
318 in PPG signals based on statistics analysis. In: 2017 29th Chi-  
319 nese Control and Decision Conference (CCDC); 2017; Nan-  
320 jing, China. IEEE; 2017; Available from: [https://doi.org/10.1109/](https://doi.org/10.1109/CCDC.2017.7979043)  
321 [CCDC.2017.7979043](https://doi.org/10.1109/CCDC.2017.7979043).
- 322 6. Elgendi M. Optimal signal quality index for photoplethys-  
323 mogram signals. *Bioengineering.* 2016;3(4):21;PMID:  
324 28952584. Available from: [https://doi.org/10.3390/](https://doi.org/10.3390/bioengineering3040021)  
325 [bioengineering3040021](https://doi.org/10.3390/bioengineering3040021).
- 326 7. Li Q, Clifford GD. Dynamic time warping and machine learning  
327 for signal quality assessment of pulsatile signals. *Physiol Meas.*  
328 2012;33(9):1491;PMID: 22902950. Available from: [https://doi.](https://doi.org/10.1088/0967-3334/33/9/1491)  
329 [org/10.1088/0967-3334/33/9/1491](https://doi.org/10.1088/0967-3334/33/9/1491).
- 330 8. Esgalhado F, Fernandes B, Vassilenko V, Batista A, Russo S. The  
331 application of deep learning algorithms for PPG signal pro-  
332 cessing and classification. *Computers.* 2021;10(12):158; Avail-  
333 able from: <https://doi.org/10.3390/computers10120158>.

9. Zhang T, Fu C. Application of improved VMD-LSTM 334  
335 model in sports artificial intelligence. *Comput Intell Neu-*  
336 *rosoci.* 2022;2022:1-9;PMID: 35875744. Available from:  
337 <https://doi.org/10.1155/2022/3410153>.
10. Huang NE, Shen Z, Long SR, Wu MC, Shih HH, Zheng Q, et 338  
339 al. The empirical mode decomposition and the Hilbert spec-  
340 trum for nonlinear and non-stationary time series analysis.  
341 *Proc R Soc Lond A Math Phys Eng Sci.* 1998;454(1971):903-  
342 95; Available from: <https://doi.org/10.1098/rspa.1998.0193>.
11. Dragomiretskiy K, Zosso D. Variational mode decomposition. 343  
344 *IEEE Trans Signal Process.* 2013;62(3):531-44; Available from:  
345 <https://doi.org/10.1109/TSP.2013.2288675>.
12. Luu TT, et al. Amplitude percentage index study for beam 346  
347 vibration signal analysis based on EEMD. *J Eng Sci Technol.*  
348 2022;17(6):3800-14;.
13. Wang S, McDermott MB, Chauhan G, Ghassemi M, Hughes MC, 349  
350 Naumann T. Mimic-extract: A data extraction, preprocessing,  
351 and representation pipeline for MIMIC-III. In: *Proceedings of*  
352 *the ACM Conference on Health, Inference, and Learning; 2020;*  
353 *Chicago, IL, USA. ACM; 2020. p. 222-35; Available from: https://doi.org/10.1145/3368555.3384469.*  
354
14. Cheng P, Chen Z, Li Q, Gong Q, Zhu J, Liang Y. Atrial fib- 355  
356 rillation identification with PPG signals using a combina-  
357 tion of time-frequency analysis and deep learning. *IEEE Ac-*  
358 *cess.* 2020;8:172692-706; Available from: [https://doi.org/10.](https://doi.org/10.1109/ACCESS.2020.3025374)  
359 [1109/ACCESS.2020.3025374](https://doi.org/10.1109/ACCESS.2020.3025374).



# Loại bỏ nhiễu tín hiệu PPG thông qua phân giải chế độ biến đổi và biến đổi Hilbert

Thái Thành Trung, Lưu Thanh Tùng\*, Phan Khánh Duy



Use your smartphone to scan this QR code and download this article

## TÓM TẮT

Tín hiệu PPG cho thấy nhiều triển vọng như một kỹ thuật không xâm lấn trong các ứng dụng khác nhau. Tuy nhiên, để sử dụng hiệu quả tín hiệu này trong các tình huống thực tế, cần phải xử lý cẩn thận để nhận diện và khắc phục các nhiễu trong tín hiệu photo-plethysmography (PPG). Trong số các phương pháp đã được khám phá, việc tích hợp phổ thời gian-tần số với mô hình học sâu kết hợp, chẳng hạn như mô hình mạng nơ-ron tích chập – bộ nhớ dài ngắn hạn (CNN-LSTM), đã nổi lên như một phương pháp đầy hứa hẹn. Tuy nhiên, các phương pháp phổ biến thường dựa vào các thuật toán Fourier để trích xuất phổ thời gian-tần số, vốn dễ gặp vấn đề rò rỉ năng lượng. Để khắc phục hạn chế này, các phương pháp phân giải như Phân Giải Chế Độ Biến Đổi (VMD) kết hợp với biến đổi Hilbert cung cấp một giải pháp hấp dẫn. Trong nghiên cứu này, chúng tôi đề xuất một thuật toán mới sử dụng VMD và biến đổi Hilbert để trích xuất phổ thời gian-tần số làm đặc trưng cho mô hình mạng nơ-ron tích chập (CNN). Không giống như các nghiên cứu sử dụng phổ thời gian-tần số dựa trên Fourier và mô hình kết hợp CNN-LSTM, cách tiếp cận này áp dụng một kiến trúc đơn giản hơn, chỉ dựa vào mô hình CNN. Sự đơn giản này nhờ vào hiệu quả của VMD và biến đổi Hilbert trong việc trích xuất đặc trưng, giúp quá trình tính toán trở nên tinh gọn mà không giảm độ chính xác. Đáng chú ý, phương pháp của chúng tôi đạt được kết quả hiệu suất cao, với độ chính xác, độ chính xác và độ nhớ tương ứng là 0.91, 0.95, 0.88 trên bộ dữ liệu MIMICIII. Những kết quả này nhấn mạnh tính bền vững và hiệu quả của phương pháp đề xuất của chúng tôi, mở ra các hướng đi đầy hứa hẹn cho việc sử dụng tín hiệu PPG trong các ứng dụng y sinh học đa dạng. Bằng cách kết hợp các kỹ thuật xử lý tín hiệu tiên tiến với các mô hình học sâu, cách tiếp cận của chúng tôi góp phần vào sự tiến bộ của xử lý tín hiệu y sinh không xâm lấn, có tiềm năng trong giám sát và chẩn đoán sức khỏe.

**Từ khóa:** tín hiệu photo-plethysmography, xử lý tín hiệu photo-plethysmography

Bộ môn máy xây dựng và nâng chuyển,  
Khoa Cơ khí, Trường Đại học Bách Khoa  
– Đại học Quốc Gia TP.HCM, Việt Nam

## Liên hệ

**Lưu Thanh Tùng**, Bộ môn máy xây dựng và  
nâng chuyển, Khoa Cơ khí, Trường Đại học  
Bách Khoa – Đại học Quốc Gia TP.HCM, Việt  
Nam

Email: luuthanhtung2002@gmail.com

## Lịch sử

- Ngày nhận: 03-3-2024
- Ngày chấp nhận: 04-7-2024
- Ngày đăng:

## DOI:



## Bản quyền

© ĐHQG Tp.HCM. Đây là bài báo công bố  
mở được phát hành theo các điều khoản của  
the Creative Commons Attribution 4.0  
International license.



**Trích dẫn bài báo này:** Trung T T, Tùng L T, Duy P K. Loại bỏ nhiễu tín hiệu PPG thông qua phân giải chế độ biến đổi và biến đổi Hilbert. *Sci. Tech. Dev. J. - Eng. Tech.* 2024; ():1-1.